

Crystal structure of the WFIKKN2 follistatin domain reveals insight into how it inhibits growth differentiation factor 8 (GDF8) and GDF11

Jason C. McCoy¹, Ryan G. Walker^{1, #}, Nathan H. Murray^{1, \$}, Thomas B. Thompson^{1, *}.

¹From the department of Molecular Genetics, Biochemistry and Microbiology, University of Cincinnati, College of Medicine, Cincinnati, Ohio 45267.

Running Title: WFIKKN2 Follistatin domain structure.

[#]Present address: Department of Stem Cell and Regenerative Biology, Harvard University, Cambridge, Massachusetts, MA 02138

^{\$}Present address: Department of Biochemistry, University of Wisconsin–Madison, Madison, WI 53706, USA

^{*}To whom correspondence should be addressed: Thomas B. Thompson: Department of Molecular Genetics, Biochemistry, and Microbiology, University of Cincinnati, Cincinnati OH 45267.
Tom.Thompson@uc.edu; Tel. (513)-558-4517

Keywords: GDF8, Myostatin, GDF11, WFIKKN, follistatin, antagonism, X-ray crystallography, structural biology, tissue homeostasis, muscle development

Abstract

Growth differentiation factor 8 (GDF8), a.k.a. myostatin, and GDF11 are closely related members of the transforming growth factor β (TGF- β) family. GDF8 strongly and negatively regulates skeletal muscle growth, and GDF11 has been implicated in various age-related pathologies such as cardiac hypertrophy. GDF8 and GDF11 signaling activities are controlled by the extracellular protein antagonists follistatin, follistatin-like 3 (FSTL3), and WAP, follistatin/kazal, immunoglobulin, Kunitz and netrin domain containing (WFIKKN). All of these proteins contain a follistatin domain (FSD) important for ligand binding and antagonism. Here, we investigated the structure and function of the FSD from murine WFIKKN2 and compared it with the FSDs of follistatin and FSTL3. Using native gel shift and surface plasmon resonance analyses, we determined that the WFIKKN2 FSD can interact with both GDF8 and GDF11 and block their interactions with the type II receptor activin A receptor type 2B (ActRIIB). Further, we solved the crystal structure of the WFIKKN2 FSD to 1.39 Å resolution and identified surface-exposed residues that when substituted with alanine, reduce antagonism of GDF8 in full-length WFIKKN2. Comparison of the WFIKKN2 FSD with those of

follistatin and FSTL3 revealed differences in both the FSD structure and position of residues within the domain that are important for ligand antagonism. Taken together, our results indicate that both WFIKKN and follistatin utilize their FSDs to block the type II receptor but do so via different binding interactions.

Introduction

Growth Differentiation Factor 8 (GDF8), also known as Myostatin, is a member of the TGF- β superfamily of ligands(1). GDF8 is a potent negative regulator of skeletal muscle growth where genetic deletion results in a hyper-muscular phenotype(2, 3). In the adult animal, several studies have established that downregulation, or inhibition, of GDF8 induces muscle hypertrophy(2–7). In contrast, transgenic overexpression of GDF8 causes muscle wasting, consistent with the idea that certain tumors increase GDF8 levels and contribute to cancer cachexia(8–11). GDF11, which shares 90% identity at the amino acid level, has distinct functions and is important for proper anterior-posterior patterning(12, 13). Recent evidence supports a beneficial role of GDF11 in neurogenesis, however excessive treatment of mice with GDF11 results in muscle wasting, similar to GDF8(14–16). Given that GDF8 and GDF11 have prominent roles in tissue homeostasis, there has

been a strong interest in developing therapeutics that modulate their signaling, especially ones that aim to boost muscle by targeting GDF8 in muscle-related pathologies(17–22).

To signal, TGF- β ligands binds to, and coordinate the assembly of two type II and two type I serine-threonine kinase receptors(1). GDF8 and GDF11 signal by using a select combination of receptors; ActRIIA or ActRIIB (type II) coupled with Alk4 or Alk5 (type I)(23–25). Ligand activity is selectively controlled by extracellular protein antagonists that bind to ligands and interfere with receptor binding. Although TGF- β ligands are structurally similar, antagonists have variable sizes and domain architectures(23, 26–30). This structural diversity allows different antagonists to selectively inhibit subsets of TGF- β family members. Over the years, structural studies have provided insight into how different antagonists can adopt different mechanisms to bind and neutralize ligands. However, it appears that in most cases antagonists block both the type I and type II receptor binding interfaces(23, 29–32).

A number of antagonists have been shown to bind and block GDF8 signaling, including follistatin splice variants follistatin288 (Fs288) and follistatin315 (Fs315), FSTL3 (follistatin-like 3), decorin, and WFIKKN(23, 26–28, 33, 34). While follistatin and FSTL3 antagonize multiple ligands including activin A and activin B, WFIKKN is exceptionally specific for GDF8 and GDF11(26, 34–36).

WFIKKN is named from the conserved multi-domain architecture - Whey Acidic Protein (WAP), Follistatin domain (FSD), Immunoglobulin domain (Ig), two tandem Kunitz (K1, K2) domains and a Netrin (N) domain (**Figure 1a**). Most animals have two related versions of WFIKKN, WFIKKN1 and WFIKKN2, which share 56% identity(37, 38). Differences in potency and binding stoichiometry have previously been reported where WFIKKN2 has an IC_{50} of 0.26nM for GDF8 antagonism and is nearly 100-fold more potent than WFIKKN1(38). In addition, WFIKKN2 forms a 1:1 complex with GDF8/11 (1 WFIKKN2 and 1 ligand dimer), whereas WFIKKN1 forms a 2:1 complex. Interestingly, removing the Kunitz 2 and Netrin domains both reduces the potency of WFIKKN2 (IC_{50} =7.2nM) and shifts the binding stoichiometry to that of full length WFIKKN1(38). While

multiple domains are thought to interact with GDF8 and GDF11, previous studies have determined that the FSD plays a significant role in antagonism(34, 38).

Follistatin domains are also functionally important for the antagonists follistatin and FSTL3. FSTL3 and follistatin contain two and three FSDs, respectively, which have been shown through multiple X-ray crystal structures to directly contact the ligand(23, 32, 39). Interestingly, each of the FSDs (FSD1-3) within follistatin/FSTL3 adopt different molecular conformations and functions differently at the ligand interface, indicating that the FSDs are not functionally redundant. In fact, biochemical experiments showed that changing the order of the FSDs can severely alter ligand binding and specificity(27, 40).

While WFIKKN selectively inhibits GDF8 and GDF11, the molecular basis for ligand selectivity has not been established. Given that WFIKKN and follistatin/FSTL3 each have FSDs important for binding, whether they exhibit unique or common ligand mechanisms has not been determined. To investigate this, we characterized the WFIKKN FSD and contrasted the binding features of the follistatin FSDs with the WFIKKN FSD. We found that the FSD of WFIKKN blocks the type II receptor binding interface similar to the FSD2 of follistatin and FSTL3. However, WFIKKN2 FSD displays different structural features, and residues that interact with the ligand that map to a different location of the FSD, indicating a different binding mode when compared to the FSDs of follistatin and FSTL3.

Results

Production of WFIKKN2 Follistatin Domain. Recombinant murine WFIKKN2 FSD, containing residues 104 to 172, was produced in bacteria. WFIKKN2 FSD protein formed inclusion bodies which were solubilized and subjected to oxidative refolding to induce disulfide bond formation. Properly folded material was purified using reverse phase chromatography as depicted in **Figure 1b**. First, Native-PAGE was used to analyze the refolded WFIKKN2 FSD and to evaluate binding interactions with GDF8. FSD alone migrated as a single band indicating the isolation of a single refolded species. Similar to previous published results, GDF8 alone does not enter the Native-PAGE and is not visible(25). Upon mixing

WFIKKN2 FSD with GDF8 an additional band appeared indicating complex formation (**Figure 1c**). Titration of GDF8 with increasing concentrations of WFIKKN2 FSD showed an increase in the complex band intensity. Analysis of the newly formed band by SDS-PAGE shows that both WFIKKN2 FSD and GDF8 are present, supporting complex formation (**Figure 1c**). Similar results were observed with GDF11 where the complex band was significantly sharper (**Figure 1d**). These results indicate that WFIKKN2 FSD is properly folded and can bind both GDF8 and GDF11, as previously implicated(34).

Comparison of WFIKKN2 FSD and WFIKKN2 Full length protein. We next wanted to compare the WFIKKN2 FSD to full-length (FL) WFIKKN2 for their ability to bind and antagonize GDF8 and GDF11. Surface plasmon resonance (SPR) was used to measure binding affinity where GDF8 and GDF11 were coupled to a CM5 SPR chip. Binding analysis was performed by injecting increasing concentrations of WFIKKN2 FL or WFIKKN2 FSD (**Figure 2a-d**). Similar to previous reports WFIKKN2 FL bound GDF8 and GDF11 with a high-affinity as demonstrated by the slow dissociation rate(34, 35). Consistent with the Native-PAGE analysis, WFIKKN2 FSD exhibited a significant interaction with GDF8 and GDF11, albeit with a much faster dissociation rate as compared to WFIKKN2 FL. The association and dissociation rate constants and equilibrium constant, K_D are reported in **Table 1**. Overall, WFIKKN2 FL exhibited a high-affinity interaction with GDF8 ($K_D=0.74\text{nM}$) and GDF11 (0.24nM) while the WFIKKN2 FSD was approximately 1000-fold weaker ($K_D=0.66\mu\text{M}$ for GDF8 and $0.12\mu\text{M}$ for GDF11). WFIKKN2 FL and WFIKKN2 FSD were able to bind TGF β 1, albeit weakly, but have no affinity for activin A, consistent with previous studies(35). We next sought to determine if the affinity of WFIKKN2 FSD for GDF8 and GDF11 was sufficient to inhibit signaling. Using a luciferase reporter assay responsive to GDF8 and GDF11, we titrated increasing concentrations of WFIKKN2 FL and WFIKKN2 FSD. While WFIKKN2 FL inhibited GDF8 and GDF11 signaling with an IC_{50} value of 0.34nM and 0.13nM , respectively, WFIKKN2 FSD exhibited a significantly reduced inhibition of GDF8 and GDF11 with an IC_{50} value of $0.85\mu\text{M}$

and $0.28\mu\text{M}$, respectively (**Figure 2d**), similar to the 1000x difference in binding affinity determined by SPR. This demonstrates that while the WFIKKN2 FSD binding affinity is severely reduced compared to full length WFIKKN2, it is still able to antagonize GDF8 and GDF11, albeit with weaker potency.

Does the WFIKKN2 FSD bind GDF8 at the type II receptor epitope? To signal, GDF8 binds the extracellular domain of the type II receptor, ActRIIB with high affinity ($K_D \sim 1\text{nM}$)(41, 42). Two ActRIIB receptors are expected to bind GDF8, or GDF11, at each knuckle region of the dimeric ligand, similar to the observed binary crystal structures of ActRIIB in complex with activin A and BMP7(43, 44). Previous studies have demonstrated that full-length WFIKKN2 interferes with type II receptor binding(26). To determine if WFIKKN2 FSD could interfere with type II receptor binding we performed a competition analysis using Native-PAGE. GDF11 mixed with WFIKKN2 FSD was titrated with increasing concentrations of the extracellular domain of ActRIIB (ActRIIB-ECD) and analyzed by Native-PAGE (**Figure 3a**). GDF11 was used for analysis since the complex bands bound to WFIKKN2 FSD and ActRIIB-ECD are more distinct than those with GDF8. Our results show that ActRIIB-ECD easily displaces WFIKKN2 FSD leading to the formation of the ActRIIB-ECD:GDF11 complex (**Figure 3a**). A higher order complex that contained all three components was not visible indicating that the WFIKKN2 FSD and ActRIIB-ECD were mutually exclusive and likely bind to the same position on the ligand. Bands corresponding to WFIKKN2 FSD:GDF11 and ActRIIB-ECD:GDF11 were excised and verified by SDS-PAGE gel under reducing conditions (**Figure 3b**). These results indicate the WFIKKN2 FSD and ActRIIB compete for the same binding interface of GDF11.

To further test the idea that WFIKKN2 FSD and ActRIIB bind GDF8 and GDF11 at similar locations competition experiments were performed using SPR. Experiments were conducted using the extracellular domain of ActRIIB fused to the Fc portion of an antibody (ActRIIB-Fc). ActRIIB-Fc was captured onto a protein A chip followed by an injection of GDF11 to form the binary ActRIIB-Fc:GDF11 complex. We next injected WFIKKN2 FSD at 500nM and observed no increase in binding,

indicating that the WFIKKN2 FSD could not bind GDF11 in the presence of ActRIIB (**Figure 3c**). Interestingly, when similar experiments were performed with WFIKKN2 FL a noticeable mass increase was observed indicating that WFIKKN2 FL was able to bind GDF11 that was already in complex with ActRIIB (**Figure 3c**).

Crystallization and Structural determination of WFIKKN2 FSD. Since the WFIKKN2 FSD can bind and antagonize GDF8 and GDF11, we next wanted to determine the molecular structure and draw comparison to the FSD of follistatin and FSTL3. The X-ray crystal structure of WFIKKN2 FSD was solved by single isomorphous replacement with anomalous scattering to 1.39 Å resolution. Data collection and refinement statistics are presented in **Table 2**. **Figure 4a** depicts the overall structure of the WFIKKN2 FSD. Similar to other FSDs, the structure contains two subdomains; an N-terminal EGF-like portion followed by a Kazal-like protease inhibitor subdomain. The EGF-like portion contains anti-parallel β -strands (β 1, β 2), whereas, the Kazal-like protease inhibitor subdomain contains a central helix (α 1) and another set of anti-parallel β -strands (β 3, β 4) that caps the Kazal subdomain. Similar to the FSDs from follistatin and FSTL3, the WFIKKN2 FSD contains 5 conserved disulfide bonds. Two are positioned in the EGF subdomain that connect the β 1 and β 2 strands (**Figure 4a**). The other three are located in the Kazal subdomain - two link the α 1 to the segment connecting the EGF and Kazal subdomains and one links β 3 to the C-terminus.

WFIKKN2 FSD mutagenesis and inhibition. Utilizing the structure, we wanted to identify residues that are important for the interaction with GDF8 and GDF11. TGF- β Ligands, including BMP2, BMP4, BMP7, activin A, activin B, GDF8 and GDF11, predominantly interact with receptors and extracellular antagonists using hydrophobic interactions(23, 45). Therefore, we hypothesized that surface exposed hydrophobic residues of WFIKKN2 FSD might be important for ligand binding and antagonism. Several surface exposed hydrophobic residues in both the EGF and Kazal subdomains were readily apparent (**Figure 4b**)(46). Residues were selected for alanine mutagenesis, including two that are positioned in the EGF domain (F109, W121) and three positioned within the Kazal subdomain (F139, F153, and I163)

(**Figure 5a**). In order to determine if these residues were important for WFIKKN2 antagonism, we generated single point mutations of the selected residues in the full length WFIKKN2. WT and mutant versions of WFIKKN2 FL were expressed in human embryonic kidney cells (HEK-293F), purified, and tested for GDF8 inhibition in a cell-based luciferase reporter assay. HEK293T-CAGA cells were treated with 0.62nM GDF8 and titrated with increasing concentrations of either purified wildtype or mutant WFIKKN2 FL (**Figure 5b**). Data were fit to a dose-response curve to determine an IC_{50} for WFIKKN2 FL and mutations. Mutations within the EGF domain (F109A and W121A) resulted in little to no change in the antagonism of GDF8. However, WFIKKN2 mutants tested within the Kazal subdomain (F139A, F153A, and I163A) all displayed weaker GDF8 inhibition. The most striking effects were seen with the mutations F139A and F153A which were 10- and 18-fold weaker than WT WFIKKN2 (**Figure 5**). Thus, the three residues that had a negative impact on GDF8 antagonism are located on the highly hydrophobic face of the WFIKKN2 FSD Kazal subdomain as shown in **Figure 4**.

Comparison of the WFIKKN2 FSD to the FSDs of Follistatin. Using the structure of WFIKKN2 FSD, we can draw structural comparisons to the different FSDs in FS288 and FSTL3. Since the FSD1 and FSD2 in both FS288 and FSTL3 share similar structures, the comparison focuses on the FSDs within FS288. The WFIKKN2 FSD and the FSDs from FS288 and FSTL3 contain a similar domain architecture with EGF and Kazal protease inhibitor subdomains, including the spacing and alignment of the 5 disulfide bonds. In addition, all of the FSDs contain two highly conserved residues, T146 and Y147 highlighted in **Figure 6a**, which are conserved in the broader Kazal domain of protease inhibitors (e.g. ovomucoids and Serine protease inhibitor Kazal-type 1)(47–49). Despite these conservations, there are differences in the relative position of the subdomains making it challenging to perform an overall alignment of the FSDs. However, the Kazal subdomains exhibit similar structures where alignment results in a root mean square of 3.1, 2.1 and 2.9 Å² for FSD1, FSD2 and FSD3 of follistatin, respectively (40 α positions), when aligned to WFIKKN2 FSD. The moderate differences of the C α positions between the Kazal

subdomains localize in the loops connecting the α 1-helix and the position of β -strands 3 and 4. Despite their similar structure, the Kazal subdomain of WFIKKN2 FSD only contains 2 of the 3 β -strands found in other FSDs (**Figure 6b**).

While the individual subdomains are structurally similar, there are significant conformational differences in the relative position of the subdomains. In retrospect, this explains why using the available FSD structures (FSD1-3) as search models failed to provide a molecular replacement solution for the WFIKKN2 FSD X-ray diffraction data. Thus, we aligned the structures using only the Kazal subdomain (**Figure 6b**). Comparison of the structures shows that different FSDs can adopt either an “open” or “closed” conformation. An open conformation is observed in FSD1 and WFIKKN2 FSD where the EGF β -strands are extended away from the Kazal domain, which creates a more linear appearance of the FSD domain. In contrast, a closed, more compact conformation is observed in FSD2 and FSD3 where the EGF domain, specifically β -strand 1, interacts with the Kazal domain. In FSD2, T178, V180, and V181 within β -strand 1 of the EGF domain form hydrophobic interactions with the Kazal subdomain (**Figure 6b**). Similarly, in FSD3, K256, L258, and F261 of β -strand 1 in the EGF domain interact with the Kazal domain. While the FSD of WFIKKN2 is in the open conformation, it should be noted that the N-terminus contains tandem glutamine residues (Q113 and Q114) that wrap back into the Kazal subdomain to interact with the α 1-helix. Residues at the interfaces of all the FSD are highly conserved across species, including Q113 and Q114, suggesting that they might serve a role to stabilize the different conformations of the FSDs.

Discussion

WFIKKN proteins are evolutionarily conserved in all vertebrates and can be found in other organisms such as sea urchins and worms(37). When compared to other extracellular protein antagonists of the TGF- β family, WFIKKN proteins are remarkably specific for the ligands GDF8 and GDF11(26, 35). While the basis for this specificity remains unknown, it is clear that the FSD plays an important role in binding and antagonism(34, 38). For example, a construct containing only the WF domains of WFIKKN2 is sufficient for antagonism of GDF8, and the FSD of WFIKKN1 has a higher

affinity for GDF8 than the Kunitz2 and Netrin domain(34, 38). Interestingly, comparing the different domains of WFIKKN2, the FSD is the most conserved domain across mammalian species, experiencing the lowest rate of substitution(37).

In other ligand antagonists, such as follistatin and FSTL3, FSDs play an important role in ligand binding and antagonism(32, 40, 50). However, whether the FSD from WFIKKN serves a similar role remains to be determined. To address this, we produced recombinant WFIKKN2 FSD and characterized its interaction with GDF8 and GDF11.

A complex between WFIKKN2 FSD and GDF8 or GDF11 was observed using Native-PAGE analysis, which SPR experiments revealed to involve sub μ M affinity interactions. Using Native-PAGE we also demonstrated that the addition of the type II receptor, ActRIIB, was able to dissociate a WFIKKN2 FSD:GDF11 complex, suggesting a direct competition between WFIKKN2 FSD and ActRIIB. Consistent with these results, SPR experiments showed that GDF11 in complex with ActRIIB-Fc was unable to bind WFIKKN2 FSD. Therefore, similar to their role in follistatin and FSTL3, the FSD of WFIKKN2 appears to block or at least compete for type II receptor binding on the ligand. However, full length WFIKKN2 retained the ability to bind the GDF11:ActRIIB-Fc complex. This interaction is likely due to other domains of WFIKKN2 associating with regions of GDF8 and GDF11 apart from the type II binding site. Thus, while the other domains of WFIKKN2 are important for potent antagonism, the WFIKKN2 FSD is sufficient to antagonize GDF8 and GDF11 by blocking type II receptor binding. Whether WFIKKN2 FSD or full-length WFIKKN2 interferes with type I receptor binding has not been resolved and is complicated by the low-affinity interaction of the type I receptor with GDF8 and GDF11(25).

To help draw comparisons to the FSD of follistatin, we solved the crystal structure of WFIKKN2 FSD. The structure reveals a similar domain architecture with an N-terminal EGF subdomain and a C-terminal Kazal subdomain as previously observed for other FSDs(23, 32, 40, 51). Using the structure, we were able to identify hydrophobic residues at the surface that contribute to GDF8 antagonism. Single point mutations within

the FSD of WFIKKN2 FL reduced the capacity to inhibit GDF8, presumably by reducing the ability of WFIKKN2 FL to interact with the type II receptor binding interface. These results are consistent with antagonists across the family which use hydrophobic interactions to engage the ligand surfaces important for binding type II receptors. However, it is possible that the residues identified could be important for interacting with other domains within WFIKKN2 FL, functioning to stabilize the WFIKKN2-ligand complex.

Comparison of WFIKKN2 FSD across 54 species reveals a high sequence identity (68%) (**Supplementary Figure S1**). Interestingly, the residues identified (F139, F153, I163) within the FSD to be are important for antagonism of GDF8 are highly conserved. Further, these residues are not conserved in other FSDs (**Figure 6**), indicating they are not necessary to the structural integrity of the Kazal subdomain. Thus, the decrease in antagonism is not likely due to a misfolded FSD within WFIKKN2. Taken together, these results support a functional rather than structural role of F139, F153 and I163 in the binding and antagonism of GDF8 and GDF11.

Interestingly, when compared to follistatin and FSTL3, WFIKKN2 interacts with the ligands through a different surface of the FSD. The WFIKKN2 FSD residues, F139, F153 and I163 are located within the Kazal subdomain, centered on the hydrophobic face of the $\alpha 1$ opposite of the N-terminal loop (**Figure 4, Figure 7**). In FSD1 and FSD2, residues that interact with the ligands are located in a completely different location of the domain, especially for FSD2 where the interaction surface is on the opposite side as compared to WFIKKN2 FSD (**Figure 7**).

While it is possible that the conformational differences observed between the EGF and Kazal subdomains of FSDs are related to crystallization, the linker region is well ordered in the crystal lattice and exhibits similar temperature factors throughout the structure suggesting the conformation of the domain is stable. Consistent with the FSD having a stable structure, the open conformation of the follistatin FSD1 was observed in both the bound and unbound state, indicating that the domain structure is not affected by ligand binding and or alternative crystallization conditions.

In addition to WFIKKN, follistatin and FSTL3, FSDs are found in several proteins with various roles in TGF- β signaling. For instance, FSDs are also found in agrin, tomoregulin and FSTL1, all of which are implicated in regulating TGF- β ligand activity(52–54). This raises the question as to the general function of the FSD and whether the domain serves a common role in ligand interactions. While the FSD in both WFIKKN and follistatin/FSTL3 both interact at the type II receptor interface, differences are readily apparent in both their structures and the placement of residues utilized for this interaction. Thus, it does not appear that the FSD represents a common binding domain, but rather a stable scaffold that allows the presentation of surface exposed hydrophobic residues that can be important for protein-protein interactions.

Given the differences in domain architecture and the differences in the position of surface residues important for ligand binding, we anticipate that the FSD of WFIKKN2 does not resemble the ligand binding scheme of any of the three FSDs of follistatin. Certainly, resolution of WFIKKN2 FSD or FL in complex with a ligand will ultimately resolve these differences and help to understand how WFIKKN specifically engages GDF8 and GDF11 over other TGF- β ligands.

Experimental procedures

WFIKKN2 FSD production and purification. Mouse WFIKKN2 FSD (residues 104-172, 97% identical to human) with a cleavable N-terminal 6x-His tag was cloned into pET28a(+) and expressed in BL21 Rosetta cells. Cells were spun down and resuspended in PBS before sonication for cell lysis. Pellets were washed two times with PBS, 0.1% TritonX100 followed by a final wash with PBS. Inclusion bodies containing the WFIKKN2 FSD were solubilized using 10mM sodium tetrathionate, 100mM sodium sulfite, 100mM Tris pH 8.5, 8M urea, and 100mM DTT. Solubilized inclusion bodies were dialyzed into 4M Urea, 50mM sodium acetate pH4.5, 100mM NaCl, 50mM Tris, 15mM imidazole and rapidly diluted into refolded buffer containing 100mM Tris pH 8.5, 150mM NaCl, 1mM EDTA, 0.1mM oxidize glutathione, 0.5mM reduced glutathione, and 0.5M arginine to a final concentration of 0.1mg/ml. After three days protein was diluted 1:5 in Ni-NTA running buffer: 50mM

Tris pH 8, 500mM NaCl, and 15mM imidazole and applied to a HisTrapTM Excel column (GE Healthcare). WFIKKN2 FSD was eluted with 500mM imidazole and dialyzed into 10mM HCl prior to separation on a C18 reverse phase column (phenomenex).

ActRIIB-ECD production and purification. ActRIIB-ECD was produced within SF+ insect cells using pFastBac expression plasmid. Purification was conducted as previously described(44). In short, ActRIIB-ECD containing a 6xHis tag is purified from SF+ condition media using a Ni-NTA affinity column. Bound protein was eluted with 20mM Tris pH 7.4, 500mM NaCl containing 500mM imidazole and subsequently applied to an S75 size exclusion column. Fractions containing the ActRIIB-ECD were pooled and used for Native-Page analysis.

Native-PAGE gel and Western blot. 3ug of GDF11/8 was mixed with WFIKKN2 FSD at different molar ratios, starting with 4:1 (WFIKKN2 FSD:GDF11/8) and WFIKKN2 FSD was serially diluted 1:2 5x for a final ratio of 0.13:1. Native-PAGE gels (12%) were run at 20°C for 140min at 110V and stained using colloidal coomassie. For staining, gels were fixed using 40% EtOH and 10% Acetic Acid for at least 1 h before washing 3x using dH₂O. A working dye solution was used containing 80% colloidal coomassie and 20% Methanol and stained overnight.

Native-PAGE to SDS-PAGE transfer. Native-PAGE gels were run as described above. However, rather than a titration, one condition was repeated in 7 lanes. One lane was cut, stained, and realigned to the unstained gel. The desired stained band was used as a guide to excise the other 6 unstained bands. Excised gel was then placed in a dialysis bag with 1mL of SDS running buffer and electro-eluted with 180V for 1h. The buffer containing the eluted band was then concentrated and subjected to SDS-PAGE under reducing conditions followed by colloidal staining as described above.

Luciferase assay. Luciferase assays were conducted in HEK293 (CAGA)₁₂ cells as previously described by our laboratory(25, 38, 55). For the assay, 20,000 cells were seeded in growth media in a 96 well format on poly-D-lysine coated plates (CAT. No. 655940 Greiner Bio-One GmbH, Germany). Cells were grown at 37°C with 5% CO₂ until reaching 75-85% confluency. Media was then

removed and treated with 100uL of serum free media containing GDF8 in the presence or absence of antagonists. GDF8 was kept at a constant concentration (0.62nM) while antagonists (WFIKKN2 FSD and Full Length) were titrated in using 1:2 dilutions. After 1day cells were lysed using 1x passive lysis buffer (E1941, Promega, USA) on a plate shaker (800rpm, 20min, 20°C). Lysates were transferred to black and white 96 well plates, 40uL of LAR (E1501 and E1960, Promega, USA) was added. Firefly luminescence was measured using the Synergy H1 Hybrid Plate Reader (BioTek). All experiments were conducted independently at least twice with all data points being done in triplicate. The concentration of antagonists at which 50% of GDF8 activity is lost or IC₅₀, was calculated using non-linear regression with variable slope using GraphPad Prism 5 software.

Surface Plasmon Resonance. SPR experiments were conducted on the Biacore T200 microfluidic system. Ligands were primary amine coupled to the GE series S CM5 sensor chip (Ca. No. BR-1005-30) using manufacture's protocols. GDF8, GDF11, activin A, and TGFβ1 at 1ug/ml was sufficient to achieve ~500 response units bound to the chip. SPR experiments were conducted in HBS-EP buffer (10mM HEPES, pH 7.4, 150mM NaCl, 3mM EDTA, 0.005% P-20 surfactant (Biacore AB)). WFIKKN2 full length or WFIKKN2 FSD was diluted in HBS-EP buffer to a concentration of 500nM then serially diluted 2-fold 10 times and applied to the chip at 15ul/min. Association was measured for 180seconds followed by 120 seconds of buffer to measure dissociation. The dissociation equilibrium constant, K_D, was calculated using Biacore T200 software using a 1:1 binding model. For the receptor binding experiments, ActRIIB-Fc at a concentration of 312.5ng/ml (~4.2nM) was immobilized on a Protein A chip. GDF11 was then applied at a concentration of 250nM for 180s. Subsequently, binding of 125nM and 500nM WFIKKN2 full-length or WFIKKN2 FSD to the receptor-ligand complex was measured.

Structural Determination and Experimental Phasing. Crystals of WFIKKN2 FSD were grown in 2.5M AmNO₃ and 0.1M NaCitrate pH 4.6 via hanging drop vapor diffusion at 4mg/ml. Rectangular crystals grew to a size of 100um x 200um. Diffraction data were collected at the

Advance photon source (APS) beamline GM/CA 23-ID-D at Argonne National Laboratory. Molecular replacement techniques for phasing were unsuccessful requiring experimental phasing via single isomorphous replacement with anomalous scattering (SIRAS). In short, crystals were soaked in 5mM KCl₄Pt for 96h before being transferred to a cryogenic solution containing mother liquor and 35% PEG 550 and flash frozen. Heavy atom positions were identified using phenix AutoSol(56, 57). Phasing and model refinement were carried out using autosol and phenix.refine(58). Model validation was performed using the program molprobity(59, 60). Coordinates are available at the Protein Data Bank, accession code 6MAA. Hydrophobicity depicted in **Figure 4** was determined using Color_H pymol script(46).

WFIKKN2 FSD and Fs288 Alignment and structural representation. Sequence alignments between WFIKKN2 FSD and other FSDs were conducted using T-Coffee(61). Structural alignments were conducted using ce-alignment within Pymol(62). Alignments were conducted between the Kazal subdomain of each FSD starting with the conserved cysteine (residue 132 in

WFIKKN2) to the end of the FSD (residues 172 in WFIKKN2). Residues used for each Fs288 are as follows, FSD1: 119-166, FSD2: 194-242, FSD3: 271-318. Supplemental sequence alignments were conducted using CLUSTAL O (1.2.4)(63).

Mutagenesis and purification full length WFIKKN2. Full Length WFIKKN2 was purified as previously described(38). In short, conditioned media from CHO cells stably expressing WFIKKN2 was collected and subjected to a butyl-sepharose and heparin columns. Elutions containing WFIKKN2 were dialyzed into 50mM Tris pH 7.4, 20mM NaCl, 1mM EDTA and applied to a MonoQ 10/100 GL column and eluted with a linear gradient of NaCl. Following Mono Q, elutions were subjected to S2000 size exclusion chromatography to obtain pure WFIKKN2. Full length WFIKKN2 was cloned into pcDNA4 mammalian expression vector and subjected to site-directed mutagenesis. WFIKKN2 mutants were transfected and produced via HEK 293F cells. Following expression, WFIKKN2 mutants were purified similar to full length WFIKKN2 produced in CHO cells.

Conflicts of Interest: Thomas B Thompson is a consultant for Acceleron Pharma. Ryan G. Walker is a co-founder, scientific advisor, and holds private equity in Elevian, a company that aims to develop medicines to restore regenerative capacity. Elevian provides sponsored research support for RGW.

Author contributions: JCM, RGW and TBT designed experiments. JCM solved the FSD structure and conducted SPR, luciferase and native page analysis. RGW conducted WFIKKN mutagenesis and luciferase assays with NHM. JCM wrote the paper with TBT.

References

1. Hinck, A. P., Mueller, T. D., and Springer, T. A. (2016) Structural biology and evolution of the TGF- β family. *Cold Spring Harb. Perspect. Biol.* **8**, a022103
2. McPherron, A. C., and Lee, S. J. (1997) Double muscling in cattle due to mutations in the myostatin gene. *Proc. Natl. Acad. Sci. U. S. A.* **94**, 12457–61
3. McPherron, A. C., Lawler, A. M., and Lee, S. J. (1997) Regulation of skeletal muscle mass in mice by a new TGF- β superfamily member. *Nature*. **387**, 83–90
4. Thomas, M., Langley, B., Berry, C., Sharma, M., Kirk, S., Bass, J., and Kambadur, R. (2000) Myostatin, a negative regulator of muscle growth, functions by inhibiting myoblast proliferation. *J. Biol. Chem.* **275**, 40235–40243
5. Lee, S.-J. (2004) Regulation of muscle mass by myostatin. *Annu. Rev. Cell Dev. Biol.* **20**, 61–86
6. Monestier, O., Brun, C., Heu, K., Passet, B., Malhouroux, M., Magnol, L., Vilotte, J. L., and Blanquet, V. (2012) Ubiquitous Gasp1 overexpression in mice leads mainly to a hypermuscular phenotype. *BMC Genomics*. **13**, 541
7. Brun, C., Périé, L., Baraige, F., Vernus, B., Bonnieu, A., and Blanquet, V. (2014) Absence of hyperplasia in Gasp-1 overexpressing mice is dependent on myostatin up-regulation. *Cell. Physiol. Biochem.* **34**, 1241–59
8. Loumaye, A., de Barsey, M., Nachit, M., Lause, P., Frateur, L., van Maanen, A., Trefois, P., Gruson, D., and Thissen, J.-P. (2015) Role of Activin A and Myostatin in Human Cancer Cachexia. *J. Clin. Endocrinol. Metab.* **100**, 2030–2038
9. Lokireddy, S., Wijesoma, I. W., Bonala, S., Wei, M., Sze, S. K., McFarlane, C., Kambadur, R., and Sharma, M. (2012) Myostatin is a novel tumoral factor that induces cancer cachexia. *Biochem. J.* **446**, 23–36
10. Zimmers, T. a, Davies, M. V, Koniaris, L. G., Haynes, P., Esquela, A. F., Tomkinson, K. N., McPherron, A. C., Wolfman, N. M., and Lee, S.-J. (2002) Induction of cachexia in mice by systemically administered myostatin. *Science*. **296**, 1486–1488
11. Costelli, P., Muscaritoli, M., Bonetto, A., Penna, F., Reffo, P., Bossola, M., Bonelli, G., Doglietto, G. B., Baccino, F. M., and Fanelli, F. R. (2008) Muscle myostatin signalling is enhanced in experimental cancer cachexia. *Eur. J. Clin. Invest.* **38**, 531–538

12. McPherron, A. C., Lawler, A. M., and Lee, S. J. (1999) Regulation of anterior/posterior patterning of the axial skeleton by growth/differentiation factor 11. *Nat. Genet.* **22**, 260–264
13. Paul Oh, S., Yeo, C. Y., Lee, Y., Schrewe, H., Whitman, M., and Li, E. (2002) Activin type IIA and IIB receptors mediate Gdf11 signaling in axial vertebral patterning. *Genes Dev.* **16**, 2749–2754
14. Lu, L., Bai, X., Cao, Y., Luo, H., Yang, X., Kang, L., Shi, M.-J., Fan, W., and Zhao, B.-Q. (2018) Growth Differentiation Factor 11 Promotes Neurovascular Recovery After Stroke in Mice. *Front. Cell. Neurosci.* **12**, 205
15. Ozek, C., Krolewski, R. C., Buchanan, S. M., and Rubin, L. L. (2018) Growth Differentiation Factor 11 treatment leads to neuronal and vascular improvements in the hippocampus of aged mice. *Sci. Rep.* **8**, 17293
16. Zimmers, T. A., Jiang, Y., Wang, M., Liang, T. W., Rupert, J. E., Au, E. D., Marino, F. E., Couch, M. E., and Koniaris, L. G. (2017) Exogenous GDF11 induces cardiac and skeletal muscle dysfunction and wasting. *Basic Res. Cardiol.* **112**, 48
17. Tsuchida, K. (2008) Targeting myostatin for therapies against muscle-wasting disorders. *Curr. Opin. Drug Discov. Devel.* **11**, 487–94
18. Smith, R. C., and Lin, B. K. (2013) Myostatin inhibitors as therapies for muscle wasting associated with cancer and other disorders. *Curr. Opin. Support. Palliat. Care.* **7**, 352–60
19. Rinaldi, F., Zhang, Y., Mondragon-Gonzalez, R., Harvey, J., Perlingeiro, R. C. R., Wallace, G., McNally, E., Hoffman, E., Brown, R., Kunkel, L., Campbell, K., Emery, A., Sinha, M., Jang, Y., Oh, J., et al. (2016) Treatment with rGDF11 does not improve the dystrophic muscle pathology of mdx mice. *Skelet. Muscle.* **6**, 21
20. Singh, P., Rong, H., Gordi, T., Bosley, J., and Bhattacharya, I. (2016) Translational Pharmacokinetic/Pharmacodynamic Analysis of MYO-029 Antibody for Muscular Dystrophy. *Clin. Transl. Sci.* **9**, 302–310
21. Mendell, J. R., Sahenk, Z., Malik, V., Gomez, A. M., Flanigan, K. M., Lowes, L. P., Alfano, L. N., Berry, K., Meadows, E., Lewis, S., Braun, L., Shontz, K., Rouhana, M., Clark, K. R., Rosales, X. Q., et al. (2015) A phase 1/2a follistatin gene therapy trial for becker muscular dystrophy. *Mol. Ther.* **23**, 192–201
22. Wagner, K. R., Fleckenstein, J. L., Amato, A. A., Barohn, R. J., Bushby, K., Escolar, D. M., Flanigan, K. M., Pestronk, A., Tawil, R., Wolfe, G. I., Eagle, M., Florence, J. M., King, W. M., Pandya, S., Straub, V., et al. (2008) A phase I/II trial of MYO-029 in adult subjects with muscular dystrophy. *Ann. Neurol.* **63**, 561–571
23. Cash, J. N., Rejon, C. A., McPherron, A. C., Bernard, D. J., and Thompson, T. B. (2009) The

- structure of myostatin:follistatin 288: insights into receptor utilization and heparin binding. *EMBO J.* **28**, 2662–76
24. Rebbapragada, A., Benchabane, H., Wrana, J. L., Celeste, A. J., and Attisano, L. (2003) Myostatin Signals through a Transforming Growth Factor β -Like Signaling Pathway To Block Adipogenesis Myostatin Signals through a Transforming Growth Factor β -Like Signaling Pathway To Block Adipogenesis. *Mol. Cell. Biology.* **23**, 7230–42
 25. Walker, R. G., Czepnik, M., Goebel, E. J., McCoy, J. C., Vujic, A., Cho, M., Oh, J., Aykul, S., Walton, K. L., Schang, G., Bernard, D. J., Hinck, A. P., Harrison, C. A., Martinez-Hackert, E., Wagers, A. J., et al. (2017) Structural basis for potency differences between GDF8 and GDF11. *BMC Biol.* **15**, 19
 26. Lee, Y.-S., and Lee, S.-J. (2013) Regulation of GDF-11 and myostatin activity by GASP-1 and GASP-2. *Proc. Natl. Acad. Sci. U. S. A.* **110**, E3713-22
 27. Sidis, Y., Mukherjee, A., Keutmann, H., Delbaere, A., Sadatsuki, M., and Schneyer, A. (2006) Biological activity of follistatin isoforms and follistatin-like-3 is dependent on differential cell surface binding and specificity for activin, myostatin, and bone morphogenetic proteins. *Endocrinology.* **147**, 3586–3597
 28. Miura, T., Kishioka, Y., Wakamatsu, J. I., Hattori, A., Hennebry, A., Berry, C. J., Sharma, M., Kambadur, R., and Nishimura, T. (2006) Decorin binds myostatin and modulates its activity to muscle cells. *Biochem. Biophys. Res. Commun.* **340**, 675–680
 29. Nolan, K., Kattamuri, C., Rankin, S. A., Read, R. J., Zorn, A. M., and Thompson, T. B. (2016) Structure of Gremlin-2 in Complex with GDF5 Gives Insight into DAN-Family-Mediated BMP Antagonism. *Cell Rep.* **16**, 2077–2086
 30. Nolan, K., and Thompson, T. B. (2014) The DAN family: modulators of TGF- β signaling and beyond. *Protein Sci.* **23**, 999–1012
 31. Kattamuri, C., Luedeke, D. M., Nolan, K., Rankin, S. A., Greis, K. D., Zorn, A. M., and Thompson, T. B. (2012) Members of the DAN family are BMP antagonists that form highly stable noncovalent dimers. *J. Mol. Biol.* **424**, 313–27
 32. Cash, J. N., Angerman, E. B., Kattamuri, C., Nolan, K., Zhao, H., Sidis, Y., Keutmann, H. T., and Thompson, T. B. (2012) Structure of myostatin·follistatin-like 3: N-terminal domains of follistatin-type molecules exhibit alternate modes of binding. *J. Biol. Chem.* **287**, 1043–53
 33. Amthor, H., Nicholas, G., McKinnell, I., Kemp, C. F., Sharma, M., Kambadur, R., and Patel, K. (2004) Follistatin complexes Myostatin and antagonises Myostatin-mediated inhibition of myogenesis. *Dev. Biol.* **270**, 19–30
 34. Kondas, K., Szlama, G., Trexler, M., Patthy, L., Kondás, K., Szláma, G., Trexler, M., and Patthy,

- L. (2008) Both WFIKKN1 and WFIKKN2 Have High Affinity for Growth and Differentiation Factors 8 and 11. *J. Biol. Chem.* **283**, 23677–23684
35. Szláma, G., Kondás, K., Trexler, M., and Patthy, L. (2010) WFIKKN1 and WFIKKN2 bind growth factors TGF β 1, BMP2 and BMP4 but do not inhibit their signalling activity. *FEBS J.* **277**, 5040–5050
 36. Hill, J. J., Qiu, Y., Hewick, R. M., and Wolfman, N. M. (2003) Regulation of Myostatin in Vivo by Growth and Differentiation Factor-Associated Serum Protein-1: A Novel Protein with Protease Inhibitor and Follistatin Domains. *Mol. Endocrinol.* **17**, 1144–1154
 37. Monestier, O., Brun, C., Cocquempot, O., Petit, D., Blanquet, V., Trexler, M., Banyai, L., Patthy, L., Hill, J., Qiu, Y., Hewick, R., Wolfman, N., Nagy, A., Trexler, M., Patthy, L., et al. (2012) GASP/WFIKKN proteins: evolutionary aspects of their functions. *PLoS One.* **7**, e43710
 38. Walker, R. G., Angerman, E. B., Kattamuri, C., Lee, Y.-S., Lee, S.-J., and Thompson, T. B. (2015) Alternative Binding Modes Identified for Growth and Differentiation Factor-associated Serum Protein (GASP) Family Antagonism of Myostatin. *J. Biol. Chem.* **290**, 7506–7516
 39. Thompson, T. B., Lerch, T. F., Cook, R. W., Woodruff, T. K., and Jardetzky, T. S. (2005) The structure of the follistatin:activin complex reveals antagonism of both type I and type II receptor binding. *Dev. Cell.* **9**, 535–543
 40. Cash, J. N., Angerman, E. B., Keutmann, H. T., and Thompson, T. B. (2012) Characterization of follistatin-type domains and their contribution to myostatin and activin A antagonism. *Mol. Endocrinol.* **26**, 1167–78
 41. Sako, D., Grinberg, A. V., Liu, J., Davies, M. V., Castonguay, R., Maniatis, S., Andreucci, A. J., Pobre, E. G., Tomkinson, K. N., Monnell, T. E., Ucran, J. A., Martinez-Hackert, E., Pearsall, R. S., Underwood, K. W., Sehra, J., et al. (2010) Characterization of the ligand binding functionality of the extracellular domain of activin receptor type IIb. *J. Biol. Chem.* **285**, 21037–48
 42. Heinecke, K., Seher, A., Schmitz, W., Mueller, T. D., Sebald, W., and Nickel, J. (2009) Receptor oligomerization and beyond: a case study in bone morphogenetic proteins. *BMC Biol.* **7**, 59
 43. Greenwald, J., Groppe, J., Gray, P., Wiater, E., Kwiatkowski, W., Vale, W., and Choe, S. (2003) The BMP7/ActRII Extracellular Domain Complex Provides New Insights into the Cooperative Nature of Receptor Assembly. *Mol. Cell.* **11**, 605–617
 44. Thompson, T. B., Woodruff, T. K., and Jardetzky, T. S. (2003) Structures of an ActRIIB:activin A complex reveal a novel binding mode for TGF-beta ligand:receptor interactions. *EMBO J.* **22**, 1555–66
 45. Walker, R. G., Poggioli, T., Katsimpardi, L., Buchanan, S. M., Oh, J., Wattrus, S., Heidecker, B., Fong, Y. W., Rubin, L. L., Ganz, P., Thompson, T. B., Wagers, A. J., and Lee, R. T. (2016)

- Biochemistry and Biology of GDF11 and Myostatin: Similarities, Differences, and Questions for Future Investigation. *Circ. Res.* 10.1161/CIRCRESAHA.116.308391
46. Eisenberg, D., Schwarz, E., Komaromy, M., and Wall, R. (1984) Analysis of membrane and surface protein sequences with the hydrophobic moment plot. *J. Mol. Biol.* **179**, 125–42
 47. Ibrahim, B. S., and Pattabhi, V. (2004) Crystal structure of trypsin–turkey egg white inhibitor complex. *Biochem. Biophys. Res. Commun.* **313**, 8–16
 48. Johansson, M. W., Keyser, P., and Soderhall, K. (1994) Purification and cDNA cloning of a four-domain Kazal proteinase inhibitor from crayfish blood cells. *Eur. J. Biochem.* **223**, 389–394
 49. Pariani, S., Contreras, M., Rossi, F. R., Sander, V., Corigliano, M. G., Simón, F., Busi, M. V., Gomez-Casati, D. F., Pieckenstain, F. L., Duschak, V. G., and Clemente, M. (2016) Characterization of a novel Kazal-type serine proteinase inhibitor of *Arabidopsis thaliana*. *Biochimie.* **123**, 85–94
 50. Lee, S.-J., Lee, Y.-S., Zimmers, T. a, Soleimani, A., Matzuk, M. M., Tsuchida, K., Cohn, R. D., and Barton, E. R. (2010) Regulation of muscle mass by follistatin and activins. *Mol. Endocrinol.* 10.1210/me.2010-0127
 51. Keutmann, H. T., Schneyer, A. L., and Sidis, Y. (2004) The Role of Follistatin Domains in Follistatin Biological Action. *Mol. Endocrinol.* **18**, 228–240
 52. Geng, Y., Dong, Y., Yu, M., Zhang, L., Yan, X., Sun, J., Qiao, L., Geng, H., Nakajima, M., Furuichi, T., Ikegawa, S., Gao, X., Chen, Y.-G., Jiang, D., and Ning, W. (2011) Follistatin-like 1 (Fstl1) is a bone morphogenetic protein (BMP) 4 signaling antagonist in controlling mouse lung development. *Proc. Natl. Acad. Sci. U. S. A.* **108**, 7058–63
 53. Patthy, L., and Nikolics, K. (1993) Functions of agrin and agrin-related proteins. *Trends Neurosci.* **16**, 76–81
 54. Chang, C., Eggen, B. J. ., Weinstein, D. C., and Brivanlou, A. H. (2003) Regulation of nodal and BMP signaling by tomoregulin-1 (X7365) through novel mechanisms. *Dev. Biol.* **255**, 1–11
 55. Walker, R. G., McCoy, J. C., Czepnik, M., Mills, M. J., Hagg, A., Walton, K. L., Cotton, T. R., Hyvönen, M., Lee, R. T., Gregorevic, P., Harrison, C. A., and Thompson, T. B. (2018) Molecular characterization of latent GDF8 reveals mechanisms of activation. *Proc. Natl. Acad. Sci. U. S. A.* **115**, E866–E875
 56. Adams, P. D., Afonine, P. V., Bunkóczi, G., Chen, V. B., Davis, I. W., Echols, N., Headd, J. J., Hung, L.-W., Kapral, G. J., Grosse-Kunstleve, R. W., McCoy, A. J., Moriarty, N. W., Oeffner, R., Read, R. J., Richardson, D. C., et al. (2010) PHENIX: a comprehensive Python-based system for macromolecular structure solution. *Acta Crystallogr. Sect. D Biol. Crystallogr.* **66**, 213–221
 57. Terwilliger, T. C., Adams, P. D., Read, R. J., McCoy, A. J., Moriarty, N. W., Grosse-Kunstleve,

- R. W., Afonine, P. V., Zwart, P. H., Hung, L.-W., and IUCr (2009) Decision-making in structure solution using Bayesian estimates of map quality: the *PHENIX AutoSol* wizard. *Acta Crystallogr. Sect. D Biol. Crystallogr.* **65**, 582–601
58. Afonine, P. V., Grosse-Kunstleve, R. W., Echols, N., Headd, J. J., Moriarty, N. W., Mustyakimov, M., Terwilliger, T. C., Urzhumtsev, A., Zwart, P. H., Adams, P. D., and IUCr (2012) Towards automated crystallographic structure refinement with *phenix.refine*. *Acta Crystallogr. Sect. D Biol. Crystallogr.* **68**, 352–367
59. Williams, C. J., Headd, J. J., Moriarty, N. W., Prisant, M. G., Videau, L. L., Deis, L. N., Verma, V., Keedy, D. A., Hintze, B. J., Chen, V. B., Jain, S., Lewis, S. M., Arendall, W. B., Snoeyink, J., Adams, P. D., Lovell, S. C., et al. (2018) MolProbity: More and better reference data for improved all-atom structure validation. *Protein Sci.* **27**, 293–315
60. Chen, V. B., Arendall, W. B., Headd, J. J., Keedy, D. A., Immormino, R. M., Kapral, G. J., Murray, L. W., Richardson, J. S., Richardson, D. C., and Richardson, D. C. (2010) MolProbity: all-atom structure validation for macromolecular crystallography. *Acta Crystallogr. D. Biol. Crystallogr.* **66**, 12–21
61. Di Tommaso, P., Moretti, S., Xenarios, I., Orobittg, M., Montanyola, A., Chang, J.-M., Taly, J.-F., and Notredame, C. (2011) T-Coffee: a web server for the multiple sequence alignment of protein and RNA sequences using structural information and homology extension. *Nucleic Acids Res.* **39**, W13–W17
62. Delano, W. L. *PyMOL: An Open-Source Molecular Graphics Tool*, [online]
https://www.ccp4.ac.uk/newsletters/newsletter40/11_pymol.pdf (Accessed September 16, 2018)
63. Larkin, M. A., Blackshields, G., Brown, N. P., Chenna, R., McGettigan, P. A., McWilliam, H., Valentin, F., Wallace, I. M., Wilm, A., Lopez, R., Thompson, J. D., Gibson, T. J., and Higgins, D. G. (2007) Clustal W and Clustal X version 2.0. *Bioinformatics.* **23**, 2947–2948

FOOTNOTES

Funding was provided by the National Institute of General Medical Sciences (NIGMS) R01 GM114640. American Heart Association Grant 12PRE11790027 to R.G.W. American Heart Association Grant 18PRE33990312 to J.C.M.

The abbreviations used are: TGF, transforming growth factor, GDF: growth and differentiation factor, WFIKKN: WAP: whey acidic protein, F: follistatin, K: kunitz, N: netrin. FSD: follistatin domain, FL: Full Length, ActRII: activin receptor II, Alk: activin like kinase, SPR: surface plasmon resonance, ECD, extra-cellular domain.

Table 1: Surface Plasmon Resonance of WFIKKN2 interactions with GDF8. Values shown represent the association constant (k_a), dissociation constant (k_d), equilibrium dissociation constant (K_D) of WFIKKN2 Full length or the FSD injected over primary amine coupled GDF8 or GDF11.

WFIKKN2	GDF8 k_a (1/Ms)	GDF8 k_d (1/s)	GDF8 K_D	GDF11 k_a (1/Ms)	GDF11 k_d (1/s)	GDF11 K_D
WFIKKN2 Full Length	3.37×10^5	2.48×10^{-4}	0.74nM	6.00×10^5	1.34×10^{-4}	0.24nM
WFIKKN2 FSD	6.9×10^3	4.6×10^{-3}	0.66 μ M	3.52×10^4	4.25×10^{-3}	0.12 μ M

Table 2: X-ray crystallographic statistic for structural determination. Overall statistics of native and heavy atom datasets for WFIKKN2 FSD structural determination. Parenthesis represent the highest resolution shell.

Data Collection	Native	K ₂ PtCl ₄
Resolution (Å)	41.80-1.39 (1.42-1.39)	41.85-1.54 (1.56-1.54)
Wavelength	0.98	1.07
# of Observations	277,020	259,934
# of Unique Reflections	21,677	29,887
# of Heavy Atom Derivatives (Pt)		9
Space Group	P4 ₃ 2 ₁ 2	P4 ₃ 2 ₁ 2
Unit Cell		
<i>a, b, c</i> (Å)	46.5, 46.5, 95.7	46.6, 46.6, 95.1
<i>α, β, γ</i> (°)	90, 90, 90	90, 90, 90
Completeness (%)	99.7 (99.8)	99.9
Redundancy	12.8	24.1
Anomalous Completeness (%)		99.9
Anomalous Redundancy		13.4
R _{meas}	0.063 (0.184)	0.239 (3.508)
R _{pim}	0.024 (0.080)	0.05 (0.943)
Mean ((I)/σ(I))	25.5 (8.7)	13.2 (1.1)
BAYES-CC		55.5 ± 15.0
FOM initial (after DM)		0.357(0.61)
Refinement		
Resolution (Å)	41.80-1.39 (1.42-1.39)	
Reflections (total/free)	21,708	
Cutoff for Refinement	F > 0σ	
R _{work} /R _{free} , %	16.45/18.01	
Atoms total/protein	770/598	
Root mean square deviations		
Bonds (Å)	0.004	
Angles (°)	0.75	
Average <i>B</i> Factors (Å ²)	17	
Amino Acids	13.97	
Ligands	25.6	
Water	32.26	
Wilson <i>B</i> Factors (Å ²)	11.5	
Ramachandran plot		
Favored (%)	98.68	
Allowed (%)	1.32	
Outliers (%)	0.00	
Clashscore	2.57	

Footnote: R_{meas}, overall measure of error between multiple measurements of a reflection within I+/I-, independent of redundancy. R_{pim}, standard error of the mean for intensity measurements within I+/I-. FOM, Figure of Merit, DM, Density Modification

$$R_{meas} = \frac{\sum_{hkl} \sqrt{\frac{n}{n-1} \sum_{j=1}^n |I_{hklj} - \langle I_{hkl} \rangle|}}{\sum_{hkl} \sum_j I_{hklj}} \quad R_{pim} = \frac{\sum_{hkl} \sqrt{\frac{1}{n-1} \sum_{j=1}^n |I_{hklj} - \langle I_{hkl} \rangle|}}{\sum_{hkl} \sum_j I_{hklj}}$$

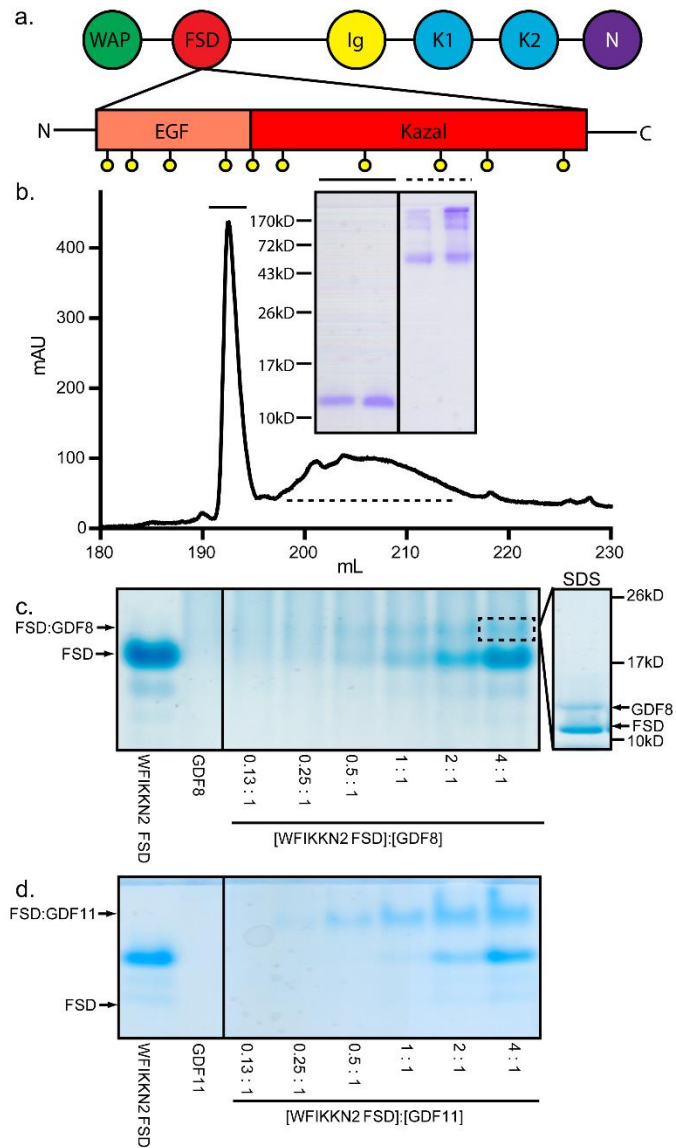


Figure 1: WFIKKN2 domain architecture and FSD purification. **a)** Domain architecture of the WFIKKN FSD. Conserved cysteines are represented as yellow spheres. **b)** Chromatograph depicting the C18 column purification of WFIKKN2 FSD. Inlet shows respective peak fractions run on an SDS-PAGE gel under non-reducing conditions. Solid line: WFIKKN2 FSD, dotted line: Misfolded FSD and contaminants **c-d)** Native-PAGE of WFIKKN2 FSD and GDF8/11 complex formation. Molar ratio of WFIKKN2:Ligand are annotated. Inlet shows the band (dotted box) that was excised and analyzed using SDS-PAGE under reducing conditions.

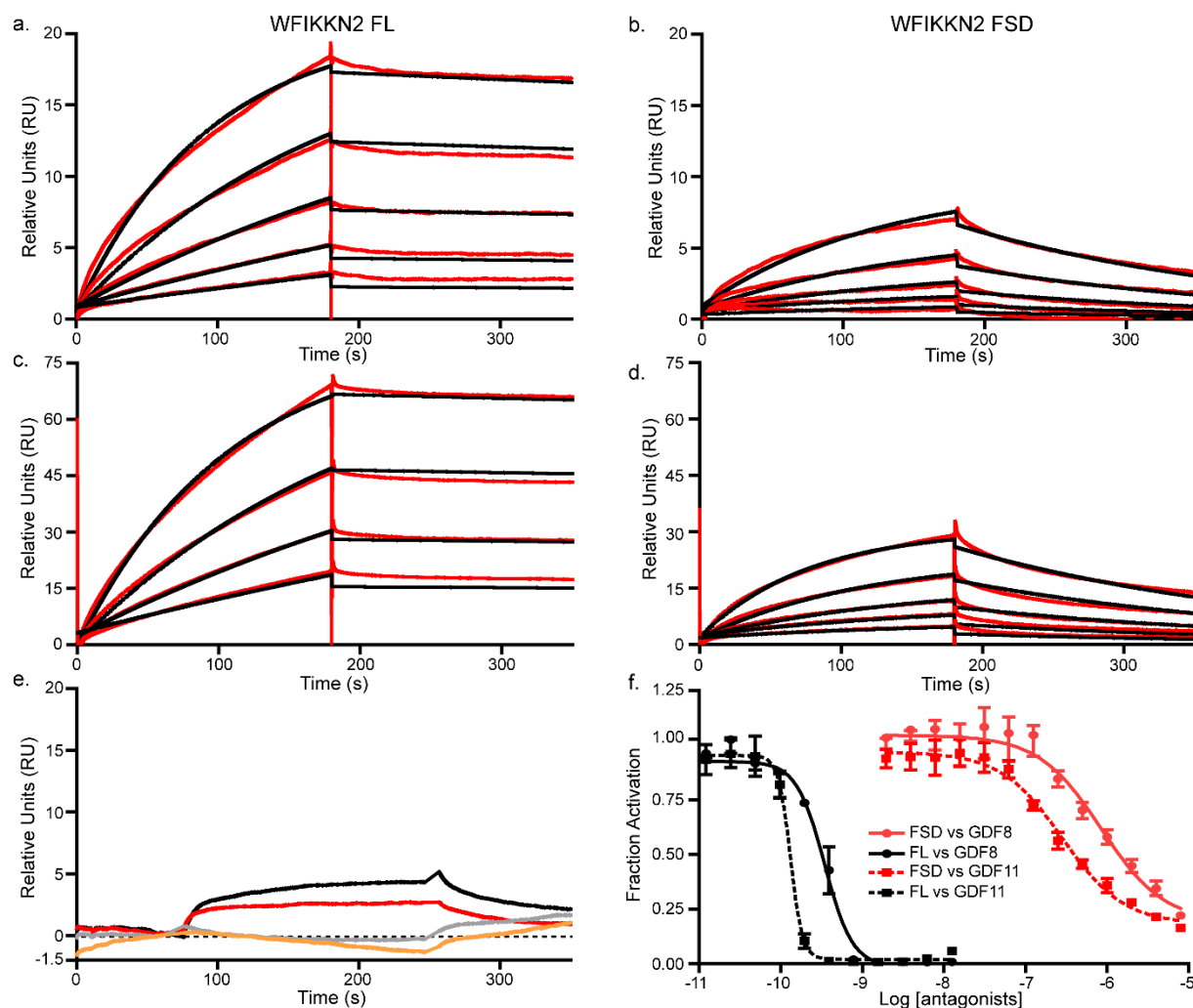


Figure 2: Binding and antagonism of WFIKKN2 FSD to GDF8. a-d) SPR of WFIKKN2 Full length (FL) and WFIKKN2 FSD over immobilized GDF8, GDF11. Red: experimental binding trace Black: data fit using a 1:1 binding model **a)** WFIKKN2 FL applied to immobilized GDF8. **b)** WFIKKN2 FSD applied to immobilized GDF8. **c)** WFIKKN2 FL applied to immobilized GDF11. **d)** WFIKKN2 FSD applied to immobilized GDF11. **e)** WFIKKN2 FL (red) or WFIKKN2 FSD (black) applied to immobilized TGF-β1. WFIKKN2 FL (grey) or WFIKKN2 FSD (orange) applied to immobilized Activin A. **f)** Luciferase assay using (CAGA)₁₂ HEK293 cells treated with GDF8/GDF11 alone or titrated with increasing concentrations of WFIKKN2 FL or WFIKKN2 FSD. Data were fit using nonlinear regression to determine an IC₅₀ and plotted as mean ± SD conducted at least twice with each point measured in triplicate.

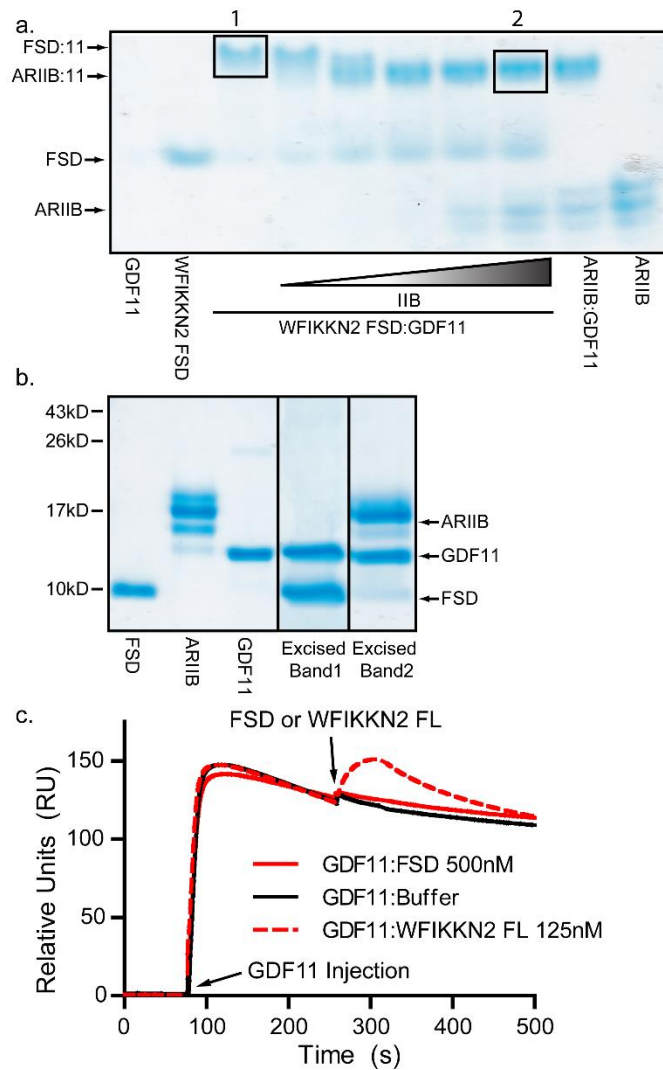


Figure 3: Competitive binding between WFIKKN2 FSD and ActRIIB to GDF11. **a)** Native-PAGE analysis using pre-formed WFIKKN2 FSD:GDF11 complex mixed with increasing amounts of ActRIIB (ARIIB). **b)** Reduced SDS gel of WFIKKN2 FSD, ARIIB, GDF11 and excised bands represented in (a) by a black box. **c)** Co-injection SPR binding experiment. First, ActRIIB-Fc was captured onto a protein A sensor chip and baseline was normalized. Next, GDF11 was injected to form the binary ActRIIB:GDF11 complex. Subsequently, WFIKKN2 FL or FSD was injected and binding to the ActRIIB:GDF11 complex was monitored.

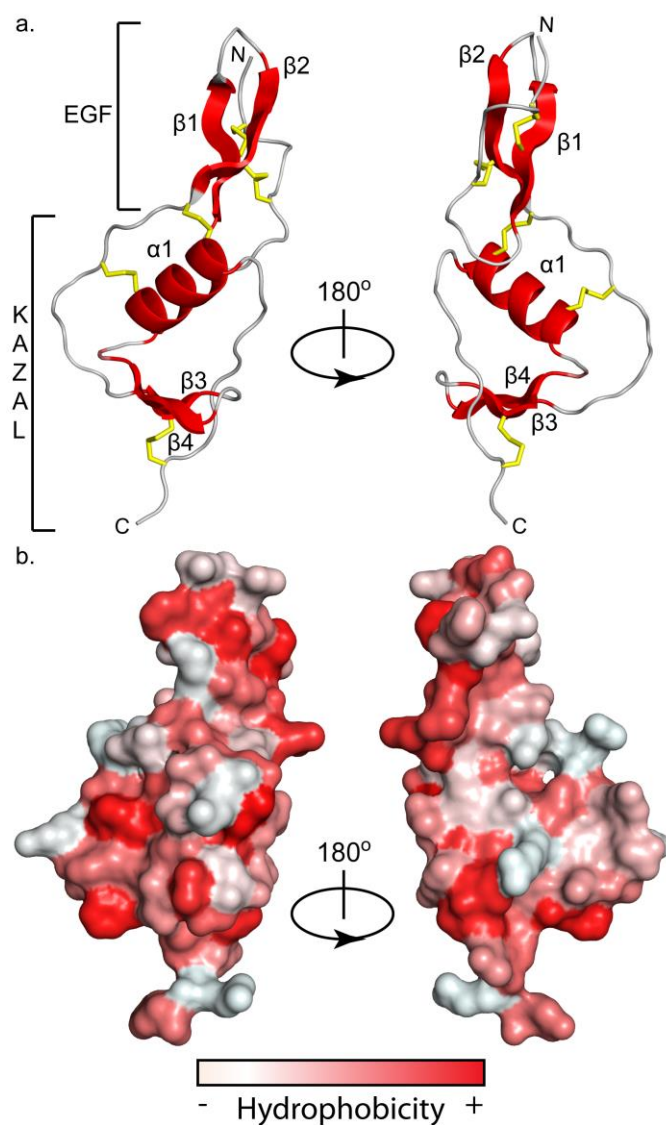


Figure 4: WFIKKN2 FSD structure and surface hydrophobicity. **a)** Ribbon diagram depicting WFIKKN2 FSD with structural components (α -helix and β -sheets) in red, flexible loops in grey, and disulfide bonds shown as yellow sticks rotated about the Y-axis 180°. **b)** Hydrophobicity of the GASP1 Fs domain surface, red being the most hydrophobic and white being the least hydrophobic using Color_H pymol script(46). Structures are in the same orientation as shown in (a).

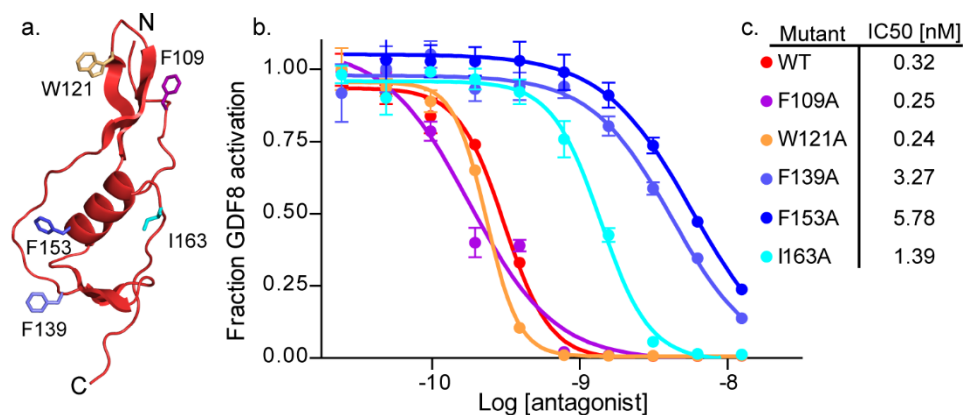


Figure 5: Full length WFIKKN2 mutant selection and inhibition **a)** Ribbon diagram of WFIKKN2 FSD, labeled sticks represent residues mutated to alanine and colored based on the inhibition curve. **b)** IC₅₀ curves generated via luciferase assay with increasing amount of WFIKKN2 mutants titrated against a constant concentration of GDF8. **c)** IC₅₀ values of mutants tested in (b) and depicted on the WFIKKN2 FSD structure in (a).

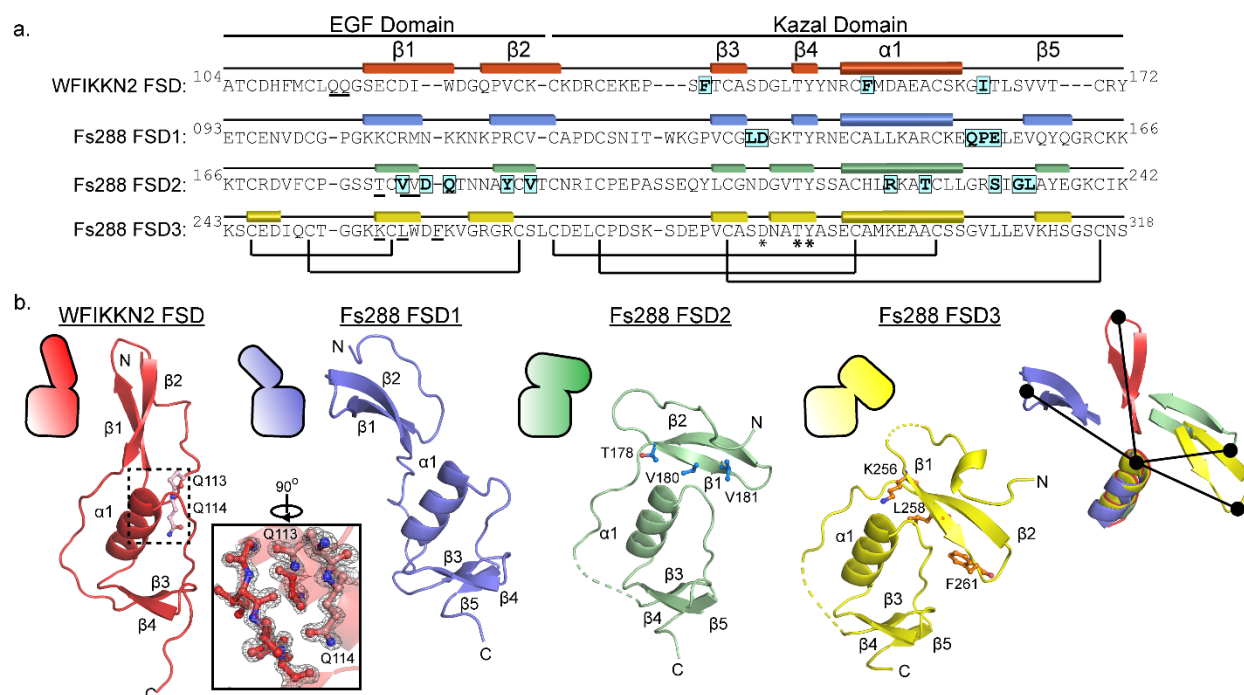


Figure 6: Comparison of WFIKKN2 FSD and Fs288 FSD1-3 a) Sequence alignment of WFIKKN2 FSD to Fs288 FSDs with the EGF and Kazal subdomains annotated, rectangles represent beta strands, cylinders represent alpha helices, black bars are conserved disulfide bonds, asterisks are conserved residues. Residues determined to be important for GDF8 binding are highlighted. Underlined residues are involved in the EGF-Kazal interaction b) WFIKKN2 FSD (Red) to FSD1 (Blue), FSD2 (Green), and FSD3 (Yellow) of Fs288 were aligned using the Kazal subdomain. (top left) Schematic representation depicting the relative orientation of the Kazal and EGF subdomains. The inset shows the 2Fo-Fc (2 σ) map of the EGF-Kazal interaction of WFIKKN2 FSD. Dotted lines represent missing segments in the crystal structures. Residues involved in the EGF-Kazal interaction are indicated in ball-and-stick. (far right) Alignment of WFIKKN2 and Fs288 FSD1-3 only depicting the alpha helix and β 1-2 of the EGF. The relative difference in orientation between the tip of the EGF domain and alpha-helix is shown by a black line.

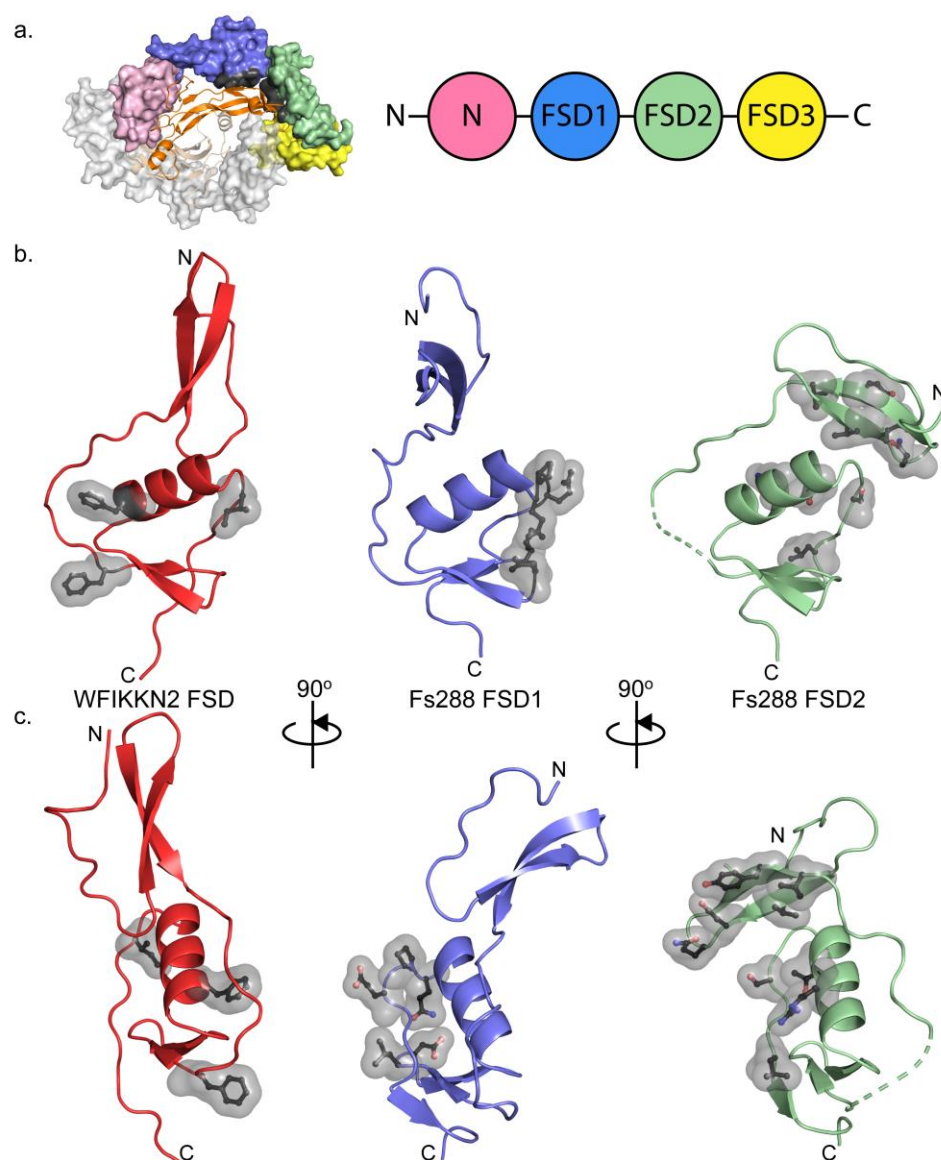


Figure 7: Binding interface of WFIKKN2 FSD is distinct from the FSDs of FS288. a) Structure of Fs288 bound to GDF8 (PDB 3HH2(23)) The central GDF8 dimer is depicted as ribbon and colored orange and wheat. One Fs288 molecule (white) is shown as a surface representation. The second FS288 molecule is shown as a surface and colored based on the schematic, FS288 FSD1-FSD2 surface that interacts with GDF8 is colored grey. **b)** WFIKKN2 FSD (red), FS288 FSD1 (blue), and FS288 FSD2 (green) are shown in similar orientation based on alignment of the Kazal subdomain. Residues within each FSD important for GDF8 antagonism are displayed. **c)** Rotation of (b) along the vertical axis by 90°.

Crystal structure of the WFIKKN2 follistatin domain reveals insight into how it inhibits growth differentiation factor 8 (GDF8) and GDF11

Jason C. McCoy, Ryan G. Walker, Nathan H. Murray and Thomas B. Thompson

J. Biol. Chem. published online February 27, 2019

Access the most updated version of this article at doi: [10.1074/jbc.RA118.005831](https://doi.org/10.1074/jbc.RA118.005831)

Alerts:

- [When this article is cited](#)
- [When a correction for this article is posted](#)

[Click here](#) to choose from all of JBC's e-mail alerts